Relationship between Equilibrium Fluctuations and Shear-Coupled Motion of Grain Boundaries

Alain Karma,[1] Zachary T. Trautt,[2] and Yuri Mishin[2]

[1]*Physics Department and Center for Interdisciplinary Research on Complex Systems, Northeastern University, Boston, Massachusetts 02115, USA*

[2]*Department of Physics and Astronomy, MSN 3F3, George Mason University, Fairfax, Virginia 22030, USA*

(Received 20 June 2012; published 27 August 2012)

We derive general analytical expressions relating the equilibrium fluctuations of a grain boundary to key parameters governing its motion coupled to shear deformation. We validate these expressions by molecular dynamics simulations for symmetrical tilt boundaries and demonstrate how they can be used to extract the misorientation dependence of the grain-boundary mobility. The results shed light on fundamental relationships between equilibrium and nonequilibrium grain-boundary properties and provide new means to predict those properties.

DOI: 10.1103/PhysRevLett.109.095501 PACS numbers: 61.72.Mm, 05.40.Ca, 61.72.Hh, 62.20.Hg

Grain boundaries (GBs) strongly influence properties of a wide range of polycrystalline materials [1,2]. In models of mechanical behavior, GBs are often treated as ''static'' geometrical obstacles to dislocation motion. This role underlies for example the classic Hall-Petch relationship predicting increased strength with decreasing grain size. However, GBs can also move in response to applied stresses. There is a growing recognition that such a motion can both influence mechanical behavior of materials and drive grain coarsening by an entirely different process than reduction in GB free energy [3–6].

The key property responsible for the GB interaction with stress is the existence of coupling between normal GB motion and shear deformation parallel to the GB plane [3,4,7,8]. This coupling is characterized by a linear relation,

$$\beta = v_{\parallel}/v_n, \tag{1}$$

between the normal GB velocity v_n and the velocity $v_{\parallel}$ of parallel grain translation. In the case of pure coupling, the coupling factor β depends only on GB bicrystallography. At high temperatures approaching the melting point, many GBs lose their coupling ability and the two velocities become uncorrelated. Due to the coupling effect, a shear stress σ applied parallel to the GB induces its normal motion. At relatively high temperatures v_n can be assumed to be proportional to the driving force F for this motion, or $v_n = M_n F$, where M_n is the GB mobility. Equating the rate of work done by the shear stress per unit GB area, $\sigma v_{\parallel}$, to the rate of free energy dissipation by normal motion, $v_n F = v_n^2/M_n$, and using the coupling relation (1), yields

$$v_n = M_n \beta \sigma. \tag{2}$$

Both atomistic simulations [3,4,7–9] and experiments [10–12] support the basic theoretical model of coupling. However, a comprehensive understanding of this effect, and the ability to predict pure coupled motion, pure sliding, or a mix of both behaviors, are still lacking. Even for pure coupling, predicting the coupling factor and mobility remains a challenge. While for symmetrical tilt GBs the misorientation dependence of β can be analytically predicted by geometric analysis [4], more recent work [13] shows that geometry alone is insufficient for predicting the coupling relation for more general, asymmetrical GBs. Furthermore, molecular dynamics (MD) simulations are generally limited to very large strain rates, making it difficult to reliably extrapolate computational predictions of M_n and β to experimental conditions.

One route to address these issues is to exploit the analysis of GB shape fluctuations to extract equilibrium and nonequilibrium GB properties from statistical averages and fluctuation-dissipation relations. While this approach is well-developed for other types of interfaces such as surfaces [14] and rough crystal-melt interfaces [15–17], its application to GBs is less developed. Previous MD studies [18,19] reported that some GBs, but not others, exhibited fluctuations of the interface height $h(x) = \sum_k A(k) e^{ikx}$ that were well described by the standard relation derived from equipartition of energy among the independent Fourier modes,

$$\langle |A(k)|^2 \rangle = \frac{k_B T}{S(\gamma + \gamma'')k^2}, \tag{3}$$

where the interface stiffness $(\gamma + \gamma'')$ is the sum of the interfacial free energy γ and its second derivative with respect to orientation of the interface normal, and $S = L_z L_x$ is the GB area assumed to have a ribbon-shape of length L_x much larger than its width L_z. Experimental studies of GB fluctuations in two-dimensional colloidal crystals reported results consistent with Eq. (3) [20]. However, previous analytical studies predicted that $\langle |A(k)|^2 \rangle \sim 1/k$ in the limit of vanishing misorientation when dislocations are well separated [21,22], which makes the extent of validity of Eq. (3) unclear. In addition, the use of fluctuation analysis to extract GB mobilities remains largely unexplored for coupled GB motion.

In this Letter we extend the analysis of GB fluctuations to the pure coupling regime and derive relations allowing

one to extract the coupling factor and GB mobility. We also generalize the GB random walk approach [23] to extract the sliding mobility $M_\parallel$ in the pure sliding regime where $v_\parallel = M_\parallel \sigma$. We present the results of MD simulations of high-temperature symmetrical tilt GBs that validate our analytical results. The MD results also shed new light on the transition from coupling to sliding and the misorientation dependence of mobility.

We first derive the equilibrium fluctuation spectrum analogous to Eq. (3) but for a perfectly coupled GB. We consider a wavy perturbation of a ribbon-shaped GB in the form $h(x) = a(k)\cos(kx)$, where the x (y) axis is chosen parallel (normal) to the unperturbed GB plane lying at $y = 0$ and z is along the tilt axis as depicted in Fig. 1. The coupling relation (1) implies that the wavy perturbation must cause the crystal lattices of each grain to translate in opposite directions with respect to each other at the peaks and troughs of the perturbed GB (green arrows in Fig. 1), generating elastic strains inside the grains. The problem of computing the GB fluctuation spectrum thus reduces to computing the elastic energy $E(k)$ of the strain field created by the wavy perturbation. We outline here the calculation of $E(k)$ for an elastically isotropic material and then state the result for cubic crystals. Details of both calculations are given in the online supplemental material [24]. The elastic energy density has the form

$$\mathcal{E} = \lambda u_{ii}^2/2 + \mu u_{ij} u_{ij}, \tag{4}$$

where λ and μ are the two Lamé coefficients and $u_{ij} = (\partial_i u_j + \partial_j u_i)/2$ is the small-strain tensor. The usual summation convention is implied. We denote by $\vec{u}^+(x, y)$ and $\vec{u}^-(x, y)$ the displacement fields in the regions above ($y > 0$) and below ($y < 0$) the unperturbed GB, respectively. These fields obey the elastostatic equation

$$\nabla^2 \vec{u}^\pm + \frac{1}{1-2\nu}\vec{\nabla}(\vec{\nabla}\cdot\vec{u}^\pm) = 0, \tag{5}$$

where ν is Poisson's ratio and $(\mu + \lambda)/\mu = 1/(1 - 2\nu)$. When broken down into x and y components, Eq. (5) yields

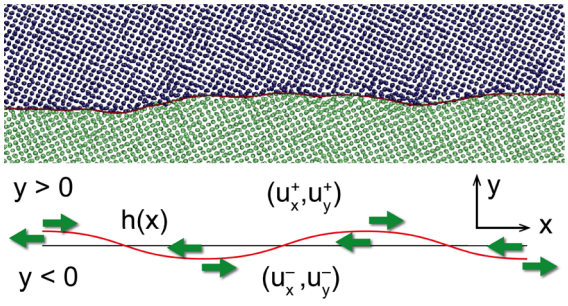

FIG. 1 (color online). Upper: typical snapshot of MD simulation where light and dark atoms (blue and green) in each grain are colored by the orientation parameter [24] used to calculate the GB normal displacement $h(x)$ (red line). Lower: schematic plot of the flat reference GB (black line) and a sinusoidal GB perturbation (red line) with green arrows showing material displacements.

two coupled scalar equations for $u_x^\pm$ and $u_y^\pm$ that must be solved in the regions $y > 0$ (+) and $y < 0$ (−) subject to several boundary conditions. These include the coupling relation (1), which translates to (cf., Fig. 1)

$$u_x^+(x, 0) - u_x^-(x, 0) = \beta h(x) = \beta a(k)\cos(kx), \tag{6}$$

the continuity of the normal displacement field $u_y^+(x, 0) = u_y^-(x, 0)$, continuity of the normal $\sigma_{yy}^+(x, 0) = \sigma_{yy}^-(x, 0)$ and tangential $\sigma_{xy}^+(x, 0) = \sigma_{xy}^-(x, 0)$ components of the traction vector at the GB, and vanishing displacement far from the GB in each grain $u_x^\pm(x, \pm\infty) = u_y^\pm(x, \pm\infty) = 0$. In writing down the continuity relations, we use the fact that it is equivalent to evaluate them at the perturbed GB position $y = h(x)$ and at $y = 0$ to linear order. Solutions of Eq. (5) that satisfy all of the above boundary conditions are found to be [24]

$$u_x^\pm = \frac{\beta a(k)}{2}\left(1 \mp \frac{ky}{2(1-\nu)}\right)e^{\mp ky}\cos(kx), \tag{7}$$

$$u_y^\pm = \frac{\beta a(k)}{4(1-\nu)}(1 - 2\nu \pm ky)e^{\mp ky}\sin(kx). \tag{8}$$

Substituting these solutions into Eq. (4) and integrating over the GB area yields the total elastic energy of the perturbation $E(k) = SC\beta^2 k a(k)^2/4$, where $C = \mu/[2(1-\nu)]$ is an effective elastic constant. Equipartition of energy implies that $E(k) = k_B T/2$, which together with the relation between complex and real amplitudes $\langle|A(k)|^2\rangle = \langle|a(k)|^2\rangle/2$ yields the final result [24]

$$\langle|A(k)|^2\rangle = \frac{k_B T}{SC\beta^2 k}. \tag{9}$$

An analogous calculation for a [001] tilt GB between cubic crystals gives the same spectrum as Eq. (9) with [24]

$$C = \frac{\bar{c}_{11} + \bar{c}_{12}}{2}\sqrt{\frac{\bar{c}_{44}(\bar{c}_{11} - \bar{c}_{12})}{\bar{c}_{11}(\bar{c}_{11} + \bar{c}_{12} + 2\bar{c}_{44})}}, \tag{10}$$

where $\bar{c}_{11}$, $\bar{c}_{12}$, and $\bar{c}_{44}$ are the elastic constants in Voigt notation with the coordinate axes parallel to the crystal axes, and where C turns out to be independent of the misorientation θ. For isotropic elasticity ($C = \mu/[2(1-\nu)]$) and small misorientation ($\theta \ll 1$ and $|\beta(\theta)| \approx \theta$), Eq. (9) reduces to the results of previous analyses where $E(k)$ was computed as the interaction energy of well separated dislocations [21,22]. However, it should be emphasized that Eq. (9) holds for arbitrary β without any restriction on misorientation under the sole assumptions that the GB exhibits pure coupled motion via Eq. (1) and that the interface stiffness is sufficiently large to suppress fluctuations linked to anisotropic interface energy.

Next, to compute the GB mobility we extend the previous analyses of time-dependent interface fluctuations [16,18] and interface random walk [23] that make use of the fluctuation-dissipation theorem. Extensions of those analyses to the pure coupling case can be found in Ref. [24]. The results show that the mobility can be extracted from computing the decay time

$\tau(k)$ of the autocorrelation function $\langle A(k,t)A^*(k,t')\rangle = \langle|A(k)|^2\rangle e^{-|t-t'|/\tau(k)}$, together with

$$M_n = \frac{S\langle|A(k)|^2\rangle}{\tau(k)k_BT}. \quad (11)$$

The GB mobility can also be obtained by measuring the Brownian-like random walk of the average GB displacement $\bar{h}(t) = (1/L_x)\int_0^{L_x} h(x,t)dx$, with

$$\langle\bar{h}^2(t)\rangle = (2M_nk_BT/S)t. \quad (12)$$

To validate the above analytical predictions, we carried out MD simulations of [001] symmetrical tilt GBs in Cu with atomic interactions modeled with the same embedded-atom potential [25] as in previous studies of coupled GB motion [4,8,9]. The simulation geometry consisted of a bicrystal with the tilt axis aligned with the z axis and the GB plane perpendicular to the y axis as in Fig. 1. Periodic boundary conditions were enforced in the x and z directions and free surfaces in the y direction, allowing the grains to freely translate parallel to the GB. The simulation block dimensions were $L_x \approx 1200$ Å, $L_y \approx 1140$ Å, and $L_z \approx 14.8$ Å with approximately 1.6×10^6 atoms. Prior to MD simulations, the ground-state GB structure was obtained using the methods described in Ref. [4]. The MD runs were about 5-ns long and implemented the canonical (NVT) ensemble at the temperature of 1200 K controlled by a Nose-Hoover thermostat.

To explore GB fluctuations in both the coupling and sliding regimes, we studied a wide enough range of tilt angles, $5.72° \le \theta \le 36.87°$, to encompass both regimes according to the previous work [4]. We define θ as misorientation between 110 directions in the grains rather than [100] as in Ref. [4]. For the lowest angle studied here, the GB is composed of cleanly separated $1/2\langle110\rangle$ dislocations, whereas at the largest angle it represents the $\Sigma5(210)$ GB. The chosen misorientation range lies within the $\langle110\rangle$ branch of coupling where the geometrically predicted "ideal" coupling factor is $\beta(\theta) = -2\tan(\theta/2)$.

Figure 2 demonstrates that the fluctuation spectrum obeys the $1/k$ behavior predicted by Eq. (9) remarkably well for the range of θ corresponding to pure coupling. In contrast, for the $\theta = 36.87°$ misorientation which is expected to exhibit pure sliding at this temperature [4], the spectrum follows the $1/k^2$ scaling law and a fit to Eq. (3) yields the physically reasonable GB stiffness $(\gamma + \gamma'') = 0.506$ J/m^2. The latter finding is consistent with the fact that, in the absence of coupling, GB fluctuations are governed by the energetic cost of creating additional GB area with orientations close to the unperturbed GB plane. Fluctuation spectra for θ in between the pure coupling and pure sliding regimes exhibit more complex variations with k without unique scaling [24].

The crossover from coupling to sliding is further examined in Fig. 3 where the MD results for $Sk\langle|A(k)|^2\rangle$ are compared to $k_BT/(C\beta^2)$ predicted by Eq. (9) with C computed from Eq. (10) using values of the elastic constants at 1200 K [24]. A good quantitative agreement is found for pure coupling. The MD values depart from the theoretical prediction at $\theta \gtrsim 25°$ when the sliding component becomes significant. Figure 3 also shows the coupling factors evaluated by two different methods: (i) from $v_\parallel/v_n$ in stress-driven simulations as in Refs. [4,7], and (ii) from linear regression between the normal GB displacement $\bar{h}(t)$ and the relative tangential translation of grains $X(t)$ during a random walk simulation. As physically expected, in the coupling regime both calculations give results very close to the ideal β. When sliding becomes significant, $v_\parallel/v_n$

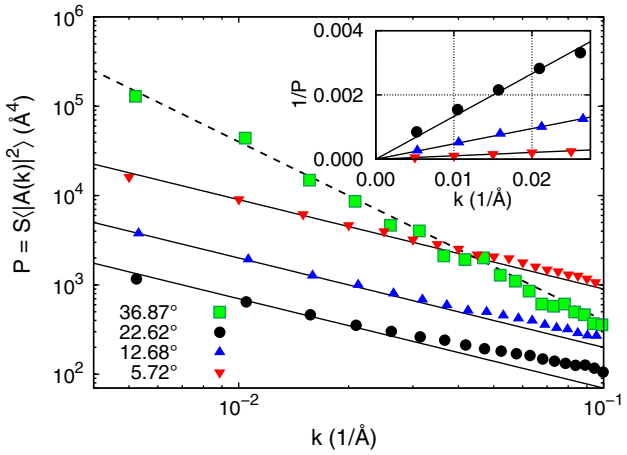

FIG. 2 (color online). Power spectrum of GB fluctuations as a function of k. Lines with slopes -1 (solid) and -2 (dashed) are shown for reference. Inset: Inverse power spectrum of GB fluctuations as a function of k with least-square linear fits to the initial part of the spectrum passing through the origin.

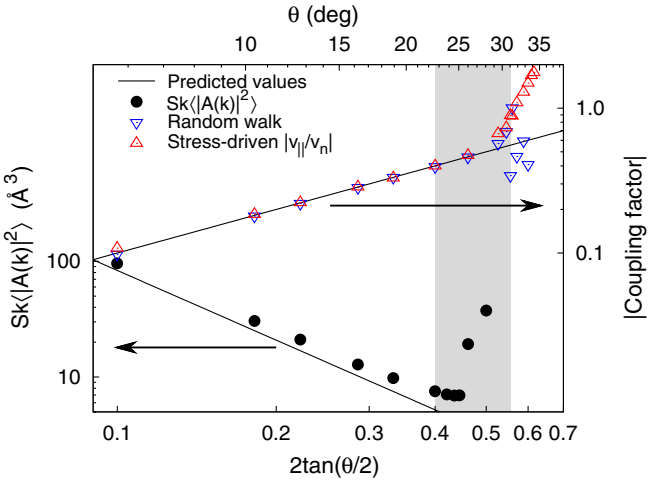

FIG. 3 (color online). Lower data: Comparison of $Sk\langle|A(k)|^2\rangle$ from MD (circles) with the prediction of Eq. (9) $k_BT/(C\beta^2)$ (solid line) plotted versus $|\beta(\theta)| = 2\tan(\theta/2)$. The gray box is the region of divergence from the prediction due to the coupling-sliding transition. Upper data: Comparison of coupling factors computed from random walk (∇) and stress-driven MD ($\triangle$) with the geometric prediction $2\tan(\theta/2)$ (solid line).

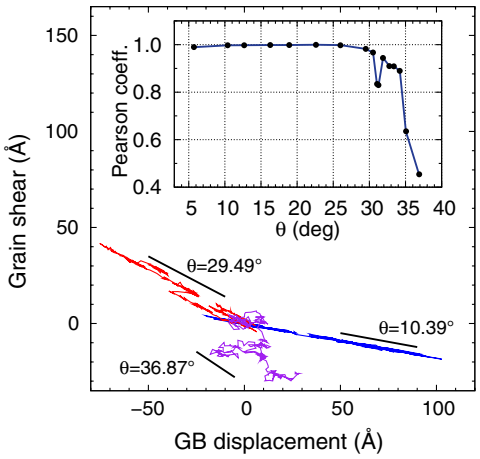

FIG. 4 (color online). Typical plots of GB displacement $\bar{h}(t)$ versus grain translation $X(t)$ during equilibrium random walk MD simulations. The line segments have the slope of the ideal coupling factors to guide the eye. At $\theta = 36.87°$ the trajectory represents uncorrelated random walk. The inset shows that the Pearson correlation coefficient between $\bar{h}(t)$ and $X(t)$ is close to unity (perfect correlation) in the coupled regime and rapidly declines due to the coupling-sliding transition.

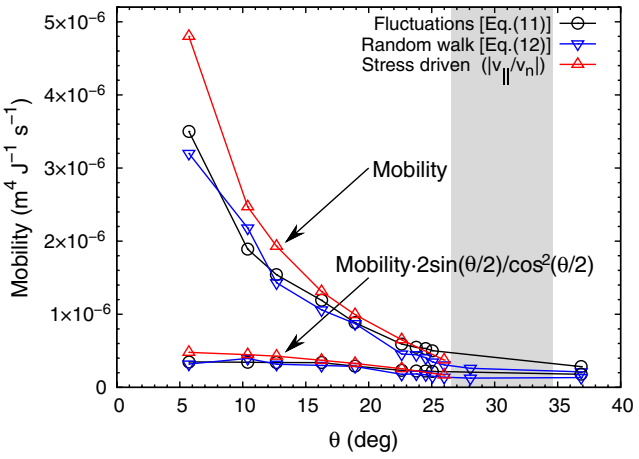

FIG. 5 (color online). GB mobility M_n computed by three different methods as a function of misorientation. The lower curves are plots of $2M_n \sin(\theta/2)/\cos^2(\theta/2)$ expected to be constant.

extracted from stress-driven simulations overshoots the ideal β because part of the grain translation velocity is now due to sliding. Figure 4 demonstrates that $\bar{h}(t)$ and $X(t)$ are strongly correlated in the coupling regime, with the regression coefficient close to β, but the correlation weakens at $\theta \gtrsim 25°$ when coupling gradually transforms to sliding. When coupling disappears ($\theta = 36.87°$), the GB performs two uncorrelated random walks in $\bar{h}(t)$ and $X(t)$.

Figure 5 summarizes the GB mobilities computed by three different methods: (i) from the GB shape fluctuations using Eq. (11), (ii) from the GB random walk using Eq. (12), and (iii) from stress-driven GB motion using Eq. (2). The first two equilibrium methods give consistent results as expected. The stress-driven M_n, which is the least accurate, tends to overestimate the mobility because very large velocities (5 m/s) were applied to create shear stresses distinguishable from thermal noise. This deviation highlights the importance of measuring GB mobility near equilibrium and avoid unrealistically large driving pressures as discussed in Refs. [2,26]. Figure 5 also shows that the mobility increases with decreasing misorientation, as was theoretically expected [3] and seen in previous MD studies [27]. Furthermore, our results confirm the relation $2M_n \sin(\theta/2)/\cos^2(\theta/2) = \text{const}$ expected assuming the conservation of dislocation content of GBs [24]. In the pure sliding regime we can also compute the sliding mobility either from $M_\parallel = v_\parallel/\sigma$ or using the random walk method giving the formula $\langle X(t)^2 \rangle = (2M_\parallel k_B T/S)t$ [24]. For the $\theta = 36.87°$ GB these two calculations give $M_\parallel = 9.1 \times 10^{-8}$ m^4/(J s) and $M_\parallel = 6.4 \times 10^{-8}$ m^4/(J s), respectively, again highlighting the importance of near-equilibrium measurements of mobility.

While the present work elucidates the fundamental link between GB fluctuations and linear response to shear for the pure coupling and pure sliding regimes, the transition between those regimes warrants further study.

This work was supported by US DOE Grants No. DE-FG02-07ER46400 (A. K) and No. DE-FG02-01ER45871 (Z. T. T and Y. M).

[1] A. P. Sutton and R. W. Balluffi, *Interfaces in Crystalline Materials* (Clarendon Press, Oxford, 1995).
[2] Y. Mishin, M. Asta, and J. Li, Acta Mater. **58**, 1117 (2010).
[3] J. W. Cahn and J. E. Taylor, Acta Mater. **52**, 4887 (2004).
[4] J. W. Cahn, Y. Mishin, and A. Suzuki, Acta Mater. **54**, 4953 (2006).
[5] T. J. Rupert, D. S. Gianola, Y. Gan, and K. J. Hemker, Science **326**, 1686 (2009).
[6] J. A. Sharon, P. C. Su, F. B. Prinz, and K. J. Hemker, Scr. Mater. **64**, 25 (2011).
[7] V. A. Ivanov and Y. Mishin, Phys. Rev. B **78**, 064106 (2008).
[8] Z. T. Trautt and Y. Mishin, Acta Mater. **60**, 2407 (2012).
[9] Y. Mishin, A. Suzuki, B. P. Uberuaga, and A. F. Voter, Phys. Rev. B **75**, 224101 (2007).
[10] T. Gorkaya, D. A. Molodov, and G. Gottstein, Acta Mater. **57**, 5396 (2009).
[11] F. Mompiou, D. Caillard, and M. Legros, Acta Mater. **57**, 2198 (2009).
[12] D. A. Molodov, T. Gorkaya, and G. Gottstein, J. Mater. Sci. **46**, 4318 (2011).
[13] Z. T. Trautt, A. Adland, A. Karma, and Y. Mishin, arXiv:1206.3549v1.
[14] Z. Toroczkai and E. Williams, Phys. Today **52**, No. 12, 24 (1999).
[15] J. J. Hoyt, M. Asta, and A. Karma, Phys. Rev. Lett. **86**, 5530 (2001).

[16] J. J. Hoyt, M. Asta, and A. Karma, Interface Sci. **10**, 181 (2002).
[17] M. Asta, C. Beckermann, A. Karma, W. Kurz, R. Napolitano, M. Plapp, G. Purdy, M. Rappaz, and R. Trivedi, Acta Mater. **57**, 941 (2009).
[18] S. M. Foiles and J. J. Hoyt, Acta Mater. **54**, 3351 (2006).
[19] J. J. Hoyt, Z. T. Trautt, and M. Upmanyu, Math. Comput. Simul. **80**, 1382 (2010).
[20] T. O. E. Skinner, D. G. A. L. Aarts, and R. P. A. Dullens, Phys. Rev. Lett. **105**, 168301 (2010).
[21] S. T. Chui, Phys. Rev. B **28**, 178 (1983).
[22] C. Rottman, Acta Metall. **34**, 2465 (1986).
[23] Z. T. Trautt, M. Upmanyu, and A. Karma, Science **314**, 632 (2006).
[24] See Supplemental Material at http://link.aps.org/supplemental/10.1103/PhysRevLett.109.095501 for derivations of equations and details of molecular dynamics simulations.
[25] Y. Mishin, M. J. Mehl, D. A. Papaconstantopoulos, A. F. Voter, and J. D. Kress, Phys. Rev. B **63**, 224106 (2001).
[26] C. Deng and C. A. Schuh, Phys. Rev. Lett. **106**, 045503 (2011).
[27] D. L. Olmsted, E. A. Holm, and S. M. Foiles, Acta Mater. **57**, 3704 (2009).